Spin-wave focusing induced by dipole-dipole interaction in synthetic antiferromagnets

R. A. Gallardo,[1,*] P. Alvarado-Seguel,[1] A. Kákay,[2] J. Lindner,[2] and P. Landeros[1]

[1]*Departamento de Física, Universidad Técnica Federico Santa María, Avenida España 1680, Valparaíso, Chile*

[2]*Helmholtz-Zentrum Dresden-Rossendorf, Institute of Ion Beam Physics and Materials Research, Bautzner Landstraße 400, 01328 Dresden, Germany*

(Received 14 May 2021; revised 6 September 2021; accepted 21 October 2021; published 15 November 2021)

Under certain conditions, spin waves can be channeled into a broad angular spectrum of wave vectors, where the direction of the group velocity becomes independent of those wave vectors. Such highly focused waves are called caustic waves, whose properties can be manipulated by anisotropies or chiral interactions, like the Dzyaloshinskii-Moriya interaction. In this paper, we theoretically study the focusing features of the spin waves induced by the dipole-dipole interaction in synthetic antiferromagnets. For stacked systems, the dipolar interaction causes a noticeable frequency nonreciprocity when the magnetizations in both films are antiparallelly aligned, and then the focusing properties of the spin waves are enhanced. The role of thicknesses and magnetic graduation along the film's normal are systematically analyzed. We found that the degree of focalization of the spin waves can be manipulated by increasing the layers' thickness. Also, we show that the low- and high-frequency modes exhibit different focalization properties; the low-frequency mode manifests a similar behavior to the heavy-metal/ferromagnet systems with interfacial Dzyaloshinskii-Moriya interaction, while the high-frequency one tends the generate almost reciprocal interference patterns along one axis. In the case of magnetization-graded synthetic antiferromagnets, we demonstrate that the graduation slightly influences the low-frequency mode, while the focusing and nonreciprocal dynamic properties of the high-frequency ones are notoriously altered. The theoretical calculations are compared with micromagnetic simulations, where a good agreement is found between both methods. Our results demonstrate that a synthetic antiferromagnetic system allows for controlling the propagation of spin waves, assisting in the transfer of angular momentum and energy.

DOI: 10.1103/PhysRevB.104.174417

I. INTRODUCTION

In optics, the concept of caustics is linked to enveloped rays, which can be achieved either through reflection or refraction in curved objects [1–3]. Caustics have been extensively studied in several fields of mathematics and theoretical physics [4–7], and also in the main fields of condensed matter physics, such as phononics [8–12], plasmonics [13,14], electronics [15–18], and magnonics [18–28]. In such cases, one relevant physical ingredient is the anisotropy of the system, which causes that the group velocity points in a different direction as compared with the phase velocity of the associated wave.

In the context of waves in magnetic media (spin waves), highly focused beams have been observed [18–29], where nonreciprocity is an important feature for creating and controlling caustic spin waves (SWs). Basically, the SW asymmetry causes an important modification in the isofrequency curve formed in the wave-vector space, where caustics appear at points at which its curvature is zero, resulting in a divergence in the power flow [25]. Nevertheless, even when the curvature is small, a substantial focusing of the energy can also be reached, and in such a case, the waves can be referred to as causticlike waves or focalized waves [26,28]. It was recently demonstrated that highly focalized spin waves and nonreciprocal interference patterns could be obtained by the excitation of a single point source in ferromagnet/heavy-metal alloys [25]. Such caustic waves were observed propagating to only one side of the film, which is a direct consequence of the nonreciprocal nature of the spin waves. From an application point of view, the focalized propagation of the waves turns out to be relevant for envisioned devices in the field of magnonics, where the control of the spin waves at the nanoscale is fundamental [28,30–34].

Nonreciprocal spin-wave propagation has been observed in magnetic systems with broken symmetries, where two counterpropagating waves exhibit different dynamic features (amplitude, frequency, or phase) at the same wave-vector magnitude. A great variety of magnonic structures manifest this nonreciprocal effect [34], such as heavy-metal/ferromagnet interfaces [35–41], noncentrosymmetric chiral magnets [42–47], curvilinear magnetic shells [48,49], magnetization-graded ferromagnetic films [50], ferromagnetic bilayers [32,51–60], bilayered magnonic crystals [61,62], and arrays of magnetic nanopillars coupled by dipolar interaction [63]. From the technological point of view, nonreciprocity turns out fundamental to envisioned magnonic applications, for instance, in circulators, isolators, phase shifters, and logic devices [64–68]. Indeed, under proper conditions, the nonreciprocal magnon propagation can even be forbidden in one direction, and the system may behave as a magnonic diode [58,59,65]. In

*rodolfo.gallardo@usm.cl

most of these systems, the origin of the nonreciprocity lies in the dipole-dipole interaction, while in ferromagnet/heavy-metal bilayers and noncentrosymmetric crystals, the cause of the nonreciprocity is the Dzyaloshinskii-Moriya (DM) interaction. In antiferromagnetically coupled bilayers (synthetic antiferromagnets), an appreciable nonreciprocity in frequency is observed due to the dynamic dipolar interaction [32,51–60,68]. This nonreciprocity can be comparable to the one induced by interfacial DM interaction in thin ferromagnetic (FM) layers, but it becomes more prominent for thick films [57,68]. Thus, if the nonreciprocal SW properties are notable in synthetic antiferromagnets, the focalization characteristics are expected to be remarkable.

In this paper, we study the two-dimensional propagation of the spin waves in synthetic antiferromagnets, where the asymmetry in the spin-wave dispersion causes an important degree of focalization on the spin-wave propagation. We consider two types of synthetic antiferromagnets, where first the antiparallel ground state is induced by a negative interlayer exchange interaction, and then such an antiparallel state is reached through an exchange-bias coupling. Also, the influence of magnetic graduation is studied. When the thickness of the ferromagnetic layers increases, we find that the focalization properties become more prominent. In the case of an antiparallel alignment stabilized through an exchange-bias coupling, the SW propagation presents a more focalized character compared to the FM/NM/FM trilayer, where the antiferromagnetic state is stabilized by a nonmagnetic spacer (NM). We also found that magnetic graduation slightly influences the degree of focalization of low-frequency modes, while at high frequencies, such graduation modifies the SW dispersion and, consequently, its power-flow features. Part of our results is contrasted with micromagnetic simulations evidencing a good agreement between both methods.

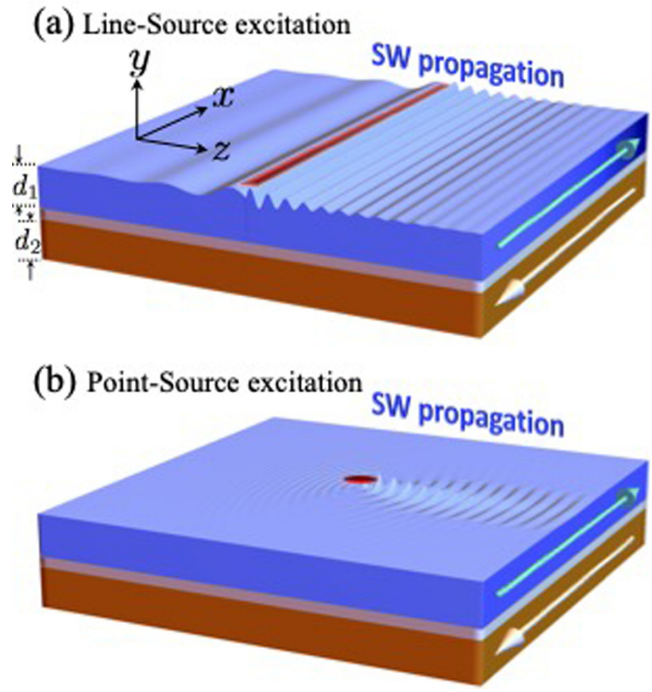

FIG. 1. Schematic representation of the spin-wave propagation in a synthetic antiferromagnet. Magnetization of the upper layer points along $+x$, while the magnetization of the bottom layer is oriented along $-x$. (a) The SW propagation is excited utilizing an external line source. (b) A point-source excitation is applied. For case (b), the highly focused SWs generated by the nonreciprocal properties of the spin waves are schematically represented.

II. THEORY

To address the magnonic properties of the system shown in Fig. 1, where the thickness of the magnetic layers can be larger than the exchange length, we will use the dynamic matrix method [69–71], which involves the subdivision of the magnetic medium into small cells, in this case, small sublayers. We have adopted this approach previously in Refs. [32,50]. Here, the main idea is to consider the thickness dependence of the magnetization dynamics by splitting the FM layer into N sublayers, labeled by μ, which are coupled via both short-range exchange and long-range dipolar interactions. In the case of the exchange, the magnetizations of two neighboring sublayers (μ and $\mu+1$) are interacting as $\epsilon^{\rm ex}_{\rm intra} = J_{\rm intra}\hat{\mathbf{M}}_\mu \cdot \hat{\mathbf{M}}_{\mu+1}$, where in the case of many divisions it can be shown that $J_{\rm intra} = 2A_{\rm ex}/d_\mu$ [32]. Here, $A_{\rm ex}$ is the exchange constant defined in the continuous limit, and d_μ is the thickness of each sublayer. Note that once the FM layer is divided into N sublayers, the dispersion of the spin waves is calculated using a convergence test that ensures the correct dynamic description of a continuous film (see details in Ref. [50]). Now, in the case of a bilayer depicted in Fig. 1, we take into account that the intralayer exchange constant is $J^{(i)}_{\rm intra}$ inside of layer i (with $i = 1, 2$), while at the interface across the nonmagnetic layer an interlayer exchange constant ($J_{\rm inter}$) is used. Thus, the interfacial nature of the interlayer exchange is accounted for and, by considering that $J_{\rm inter} < 0$, an antiparallel alignment between both magnetizations is established at low external fields. For simplicity, we introduce the interlayer exchange interaction as bulk energy, which is confined within the magnetic sublayers located next to the NM/FM interface (sublayers α and $\alpha+1$; see the Appendix for details).

The dynamics of the magnetization $\mathbf{M}^\mu$ under an effective field $\mathbf{H}^\mu_{\rm eff}$, in the absence of damping, is given by the Landau-Lifshitz (LL) equation,

$$\frac{d}{dt}\mathbf{M}^\mu = -\gamma\mu_0\mathbf{M}^\mu \times \mathbf{H}^\mu_{\rm eff}. \tag{1}$$

We are interested in the near-equilibrium propagation of the spin-wave normal modes. Assuming plane-wave solutions, we introduce the first-order perturbations $\mathbf{M}^\mu = \mathbf{M}^\mu_{\rm eq} + \mathbf{m}^\mu e^{i(\mathbf{k}\cdot\mathbf{r}-\omega t)}$ and $\mathbf{H}^\mu_{\rm eff} = \mathbf{H}^\mu_{\rm eff0} + \mathbf{h}^\mu e^{i(\mathbf{k}\cdot\mathbf{r}-\omega t)}$. Here we have assumed that the magnetization and effective field of each layer are in a uniform stable equilibrium configuration, denoted by $\mathbf{M}^\mu_{\rm eq}$ and $\mathbf{H}^\mu_{\rm eff0}$, such that they are parallel to each other. Then, at first order in the dynamic components of the magnetization and effective fields, the LL equation reduces to

$$\omega\mathbf{m}^\mu = i\gamma\mu_0\left(\mathbf{H}^\mu_{\rm eff0}\times\mathbf{m}^\mu - \mathbf{M}^\mu_{\rm eq}\times\mathbf{h}^\mu\right). \tag{2}$$

Now let us assume that the effective dynamic field $\mathbf{h}^\mu$ is a linear combination of the dynamic magnetization of every layer. Namely, $\mathbf{h}^\mu = \sum_{\nu=1}^{N}\mathbf{\Lambda}^{\mu\nu}\cdot\mathbf{m}^\nu$. It follows that the above equation defines an eigenvalue problem in a finite-dimensional

vector space, where the independent variables correspond to the spatial components of the dynamic magnetization of every layer. Then, upon selection of an appropriate basis, it is straightforward to provide a matrix representation. The only difficulty lies in obtaining an explicit formula for the operator $\mathbf{\Lambda}^{\mu\nu}$. In the Appendix, the $\mathbf{\Lambda}^{\mu\nu}$ elements of dipolar and exchange interaction are derived. Additional contributions like the external field, uniaxial anisotropy, and exchange interactions can be found in Refs. [32,50].

III. RESULTS AND DISCUSSION

In Sec. III A, we calculate the focusing properties for a typical synthetic antiferromagnet, where the antiparallel state is induced by introducing a nonmagnetic layer providing a negative interlayer exchange constant. Then, the antiparallel state of the bilayer is stabilized through an exchange-bias coupling, where a unidirectional anisotropy is induced by the interaction between the ferromagnet and an antiferromagnetic layer. In Sec. III B, the spin-wave dispersion and focusing properties of a magnetization-graded synthetic antiferromagnet are discussed. Finally, in Sec. III C, part of our results is compared with micromagnetic simulations.

A. Spin-wave dispersion and isofrequency curves

To systematically study the band structure of a synthetic antiferromagnet, we will use the standard values for Permalloy (Py) and cobalt. Specifically, the saturation magnetization of Py is $M_s^{\mathrm{Py}} = 800$ kA/m, while the exchange constant $A_{\mathrm{ex}}^{\mathrm{Py}} = 7.5$ pJ/m [72]. For cobalt the saturation magnetization and the exchange constant, respectively, are $M_s^{\mathrm{Co}} = 1400$ kA/m and $A_{\mathrm{ex}}^{\mathrm{Co}} = 28$ pJ/m [73]. We use an effective gyromagnetic ratio $\gamma = 185.6$ GHz/T for both materials, while the thickness of the nonmagnetic spacer is $s = 1$ nm. We will use an interlayer exchange constant of $J_{\mathrm{inter}} = -0.1$ mJ/m^2 that favors an antiparallel state of the magnetizations. Note that such an antiparallel equilibrium state can be stabilized at small external fields (even at zero field); therefore, in what follows, a small field of 2 mT will be used. Also, to consider the dynamic evolution of the magnetization along the thickness, the number of divisions used is $N = 26$. Because we want to enhance the nonreciprocal properties of the system, we will consider that the magnetizations are always in plane. In the case of perpendicularly magnetized FM films, the nonreciprocal properties disappear [57].

Figures 2(a), 2(b), and 2(c) show the dispersion of the SWs for $d_{1,2} = 2$, 12, and 24 nm, respectively. In such dispersions, the SWs are propagating along the z axis, while the magnetizations of both layers are pointing along $+x$ and $-x$ (see Fig. 1). We note that the spin-wave dispersion becomes asymmetric when the thicknesses of the magnetic layers increase at moderated wave vectors ($k < 20$ rad/μm), which is correlated with the dipolar interaction that also increases with the thickness and, at the same time, induces the nonreciprocity in the SW propagation [57,68] (such wave-vector range can be probed by inelastic Brillouin light scattering experiments). When both layers are in an antiparallel state, there is a propagation sense where the dynamic stray fields induced by layer 1 (2) are disposed so that they are always parallel to the local dynamic magnetization of layer 2 (1). Thus, the dynamic dipolar interaction is considerably reduced (and consequently, the frequency is reduced) when the wave propagates in some particular direction [57]. To analyze the propagation in all directions, we have generated a contour plot in k space at fixed frequencies (isofrequency curves). Figures 2(d)–(f) show the isofrequency curves (also called slowness surfaces) for the low-frequency mode (mode I) depicted as a function of the in-plane wave vector, where the group velocity vector $\mathbf{v}_g$ is denoted by the red arrows that are normal to the isofrequency curves.

Due to the degrees of freedom of the magnetization dynamics in a bilayer system, at least two modes with different oscillation phases can be excited. Furthermore, if the thicknesses of the FM layers increases, several higher modes can be observed at low frequencies, since as the thickness increases, the dynamical energy (or frequency) of such modes is reduced. Figure 2(c) shows the case where three modes are observed in the range 0–50 GHz. Nevertheless, for the sake of simplicity, we will focus on the first two low-frequency modes. In Figs. 2(g)–(i), we can see the evolution of the isofrequency curves for mode II at different film thicknesses. Here, in comparison with mode I, we can see that the focusing properties of the spin-wave propagation are entirely different. In Fig. 2(g), we observe highly focused waves that result from the flattening on the left and right parts of the slowness surfaces (see red arrows in the isofrequency curves evaluated at 16 GHz) and propagate in both $+z$ and $-z$ directions. As the thickness increases, interference patterns can be induced along both directions [see red arrows in Fig. 2(i)]. The notorious change in the curve evaluated at $f = 22$ GHz [in Fig. 2(i)] occurs since mode II hybridizes with the next high-frequency mode, so that a drastic change of the dispersion and phase occurs. This effect is also observed in the frequency shift Δf, shown in the inset of Fig. 2(c), where at about $k = 9$ rad/μm the frequency shift of mode II is drastically reduced.

According to the behavior observed for the isofrequency curves of mode I, it is clear that such curves are very similar to the one obtained in heavy-metal/ferromagnet alloys, where the interfacial DM interaction induces unidirectional caustic beams in the Damon-Eshbach geometry [25,34]. The case illustrated in Fig. 2(d), for instance, is similar to the one with a small Dzyaloshinskii-Moriya constant (D), while the case shown in Fig. 2(f) is following larger values of the DM strength. Despite these similarities, both systems present notable differences. For instance, synthetic antiferromagnets are not restricted to ultrathin films (as in heavy-metal/ferromagnet alloys). In fact, nonreciprocal and focusing properties are enhanced when the thickness increases. Also, because several paths can reach the antiferromagnetic state, there are varied alternatives to manipulate the focalization of the spin waves. In this sense, it is feasible to cancel the focalization of the waves just by changing the magnitude of the external field since the bilayer becomes parallel at high fields, and then, the system loses the nonreciprocal properties. An interesting aspect of our system is that the unidirectional steering of the waves is achieved mainly for the low-frequency mode since the high-frequency one presents focalized propagation of waves in both directions ($+z$ and $-z$). However, this focalization of the high-frequency

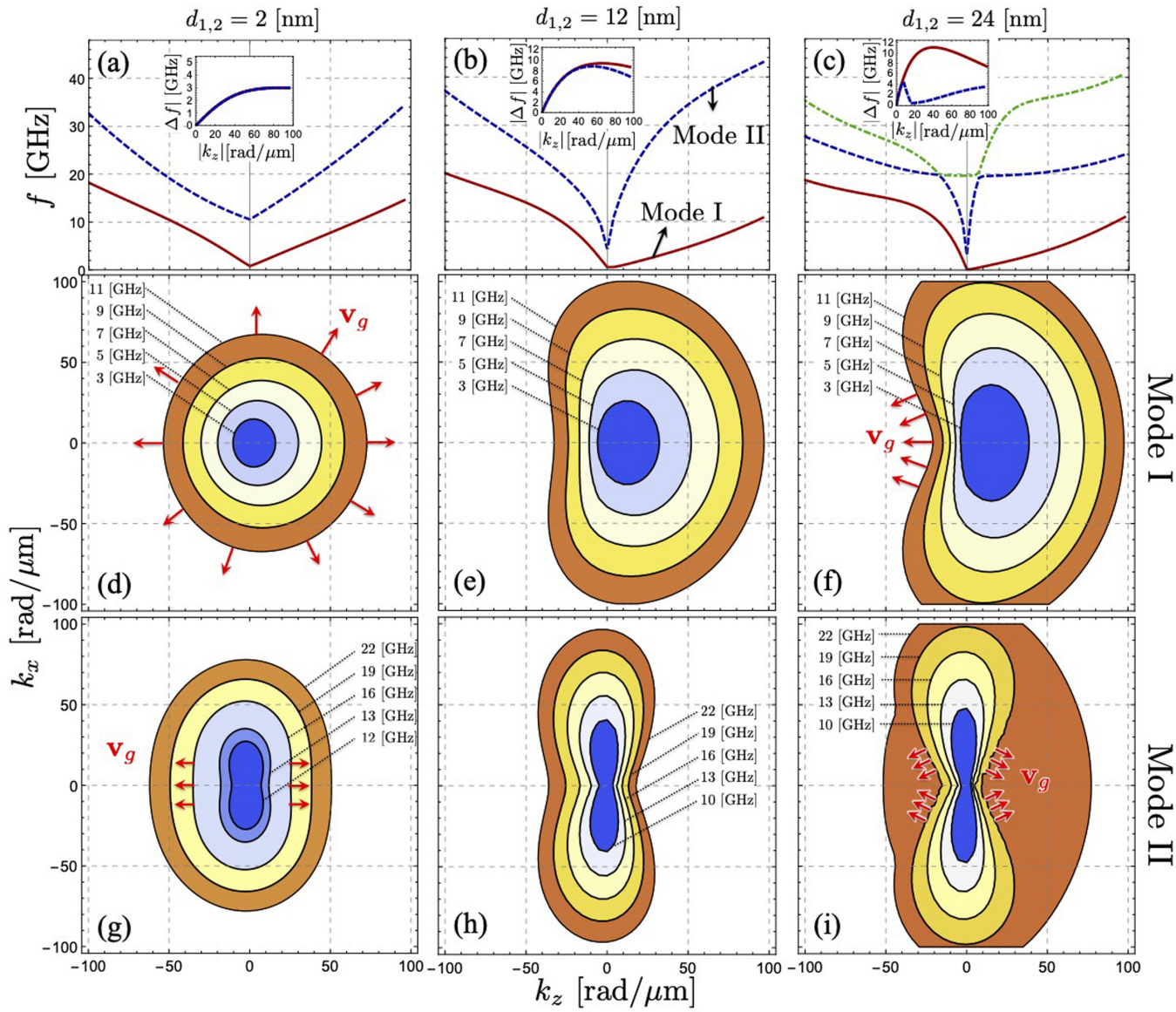

FIG. 2. (a–c) The dispersion relation of the spin waves for synthetic antiferromagnets with different thicknesses; the insets depict the frequency nonreciprocity Δf as a function of the wave vector for the first two modes, labeled as Mode I and Mode II. (d–i) Contour plots generated at a fixed frequency in k space of (d–f) mode I and (g–i) mode II. In these panels, the red arrows (that are included by hand) illustrate the orientation of the group velocity ($\mathbf{v}_g$) of the spin waves.

modes is not a trivial result, since even when the frequency shift Δf is similar in magnitude [see insets in Figs. 2(a) and 2(b)], the focusing properties have different characteristics.

To understand the formation of highly focused spin waves, we will analyze the main interactions that control the magnonic dispersion. In one isolated ferromagnetic layer where the exchange interaction dominates, the isofrequency curves will be a circle (frequency is proportional to k^2), so that the curvature is constant and consequently the energy propagates homogeneously in all in-plane directions [see Fig. 3(a)]. When the dipolar interaction is active, backward volume (BV) and Damon-Eshbach (DE) modes (wave vector parallel and perpendicular to the magnetization, respectively) have different features, and the isofrequency curve presents a variable curvature, as shown Fig. 3(b). In such a case, caustic waves may appear, where the highly focused waves propagate reciprocally [74–76]. Instead, in a synthetic antiferromagnet, the dynamic dipolar interaction induces nonreciprocity in frequency for DE modes [57]. Such nonreciprocity implies a distortion in the shape of the isofrequency curve, where (under a significant nonreciprocity) the part with the lowest wave-vector magnitude will look like a bump, as shown in Fig. 3(c). The critical point now is that the part with the bump entails a change of sign in the curvature so that there are some regions where the curvature will be zero, and therefore nonreciprocal caustic waves are formed. Thus, the strongly anisotropic dispersion induced by the dipolar interaction in a synthetic antiferromagnet can be helpful to steer spin waves, allowing a concentration of the energy. Also, since a synthetic ferromagnet can be stabilized in varied ways, there are many

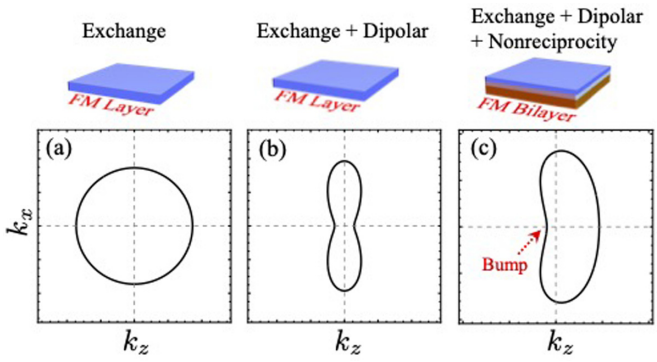

FIG. 3. Schematic representation of the isofrequency curves for a single FM layer when (a) only exchange and (b) exchange plus dipolar interaction are active. (c) The isofrequency curve is depicted for an antiferromagnetically coupled bilayer, where the dynamic dipolar coupling induces nonreciprocity in frequency.

degrees of freedom to control the causticity and the focusing of the spin waves.

In Fig. 2 we analyzed the antiparallel configuration stabilized by a negative interlayer exchange constant. Nonetheless, such an antiferromagnetic state can be stabilized by other means. In the next example, we will analyze the focusing properties when the antiferromagnetic state is reached by coupling a FM layer (Co) with an antiferromagnetic (AFM) film. In Fig. 4(a), a schematic representation of the system is shown, where the Co layer is pinned along $-x$, via an exchange-bias field $\mu_0 H_{\rm EB} = 15$ mT, while the cobalt and Permalloy films are coupled through an interlayer exchange

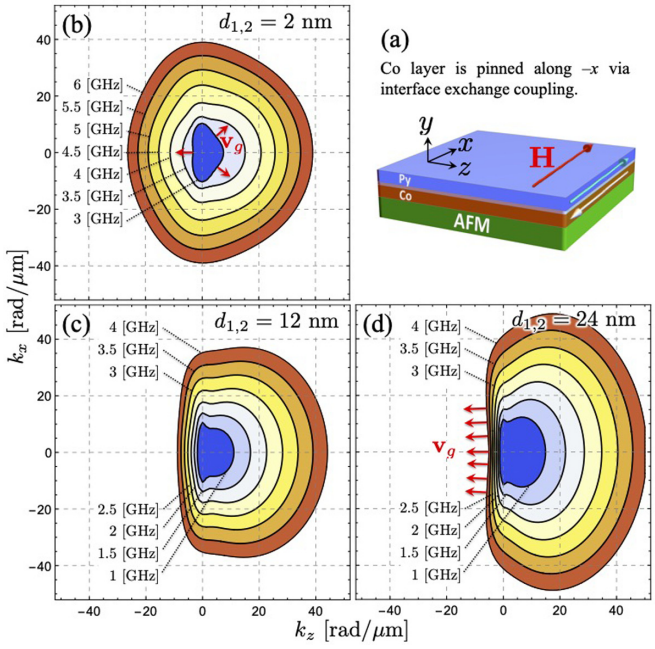

FIG. 4. (a) The schematic representation of the system is shown. The external field is applied along $+x$ so that the Py layer is also oriented along $+x$, while the Co layer is pinned along $-x$ due to the exchange-bias coupling at the FM/AFM interface. (b–d) The isofrequency curves for $d_{1,2} = 2$, 12, and 24 nm are depicted, respectively.

$J_{\rm inter} = 0.001$ mJ/m^2, so that the Py layer is almost free. Note that in this case, the interlayer exchange coupling is very different in comparison with the structure shown in Fig. 2, since here the system does not require a negative (and strong) $J_{\rm inter}$ to reach the antiferromagnetic state. Namely, even at $J_{\rm inter} = 0$, the bilayer will be in an antiferromagnetic state for small external fields. In small fields, the magnetizations of both layers are pointing along $-x$, while for high values of the external field, both magnetizations can follow the field direction ($+x$). In the intermediate case ($\mu_0 H = 2$ mT), the upper layer of Permalloy can follow the field (which is applied to $+x$), while the Co layer remains pinned along $-x$. Thus, an antiparallel alignment of the magnetizations is reached for this system. Figures 4(b)–(d) show the isofrequency curves of the first mode at three different thicknesses and evaluated at $\mu_0 H = 2$ mT. For simplicity, we show only the low-frequency mode, since the second mode (not shown) exhibits similar properties in comparison with the case illustrated in Fig. 2. Here, we can see that the evolution of the curves is different in comparison with the system studied in Fig. 2. At small thicknesses, the isofrequency curve at 3 GHz exhibits three zones with slight curvatures [see red arrows of the group velocity in Fig. 4(b)] so that we can predict three focalized waves. These focusing effects change as the frequency increases since the isofrequency curves do not have a range of wave vectors with small curvatures at significant frequencies (higher than 6 GHz). Interestingly, at larger thicknesses, the unidirectional propagation of the focused waves is allowed and slightly varies as the frequency increases [see Figs. 4(c) and 4(d)]. In Fig. 4(d), the direction of the group velocity is highlighted, where we note that highly focused beams with large wavelengths (small wave vectors) are propagating along $-z$.

B. Magnetization-graded synthetic antiferromagnets

Finally, we will consider a more particular case, where the saturation magnetization of both FM layers will be graduated in order to modify the nonreciprocity of the spin waves and their respective focalization properties. Here, to enhance the effect of the magnetic graduation, each FM film has a thickness of 60 nm. Figure 5 illustrates three different cases where the saturation magnetization varies across the thickness of the entire structure. Sublayers between $n = 1$ and 13 correspond to the bottom layer, while the sublayers labeled between $n = 14$ and 26 correspond to the upper layer. For the case without graduation, where M_s changes abruptly between two values [Fig. 5(a)], one can appreciate a notable nonreciprocity of the fundamental mode (mode I), while the upper-frequency modes have almost symmetric dispersion. An exciting aspect of the thick bilayer systems is the wide range of frequencies (0–6 GHz) where the SWs have a large group velocity at negative wave vectors, and such behavior is enhanced as the thicknesses increase [32]. Note that the magnitude of the spin-wave group velocity is about 7 km/s in the range of frequency 0–7 GHz, which is connected with the strong nonreciprocity induced by dipolar interaction in thick films. Such an order of magnitude has been previously reported in magnetic systems [77,78]. By analyzing the SW profiles (upper plots of Fig. 5), we can establish that in Fig. 5(a) the second mode (and some

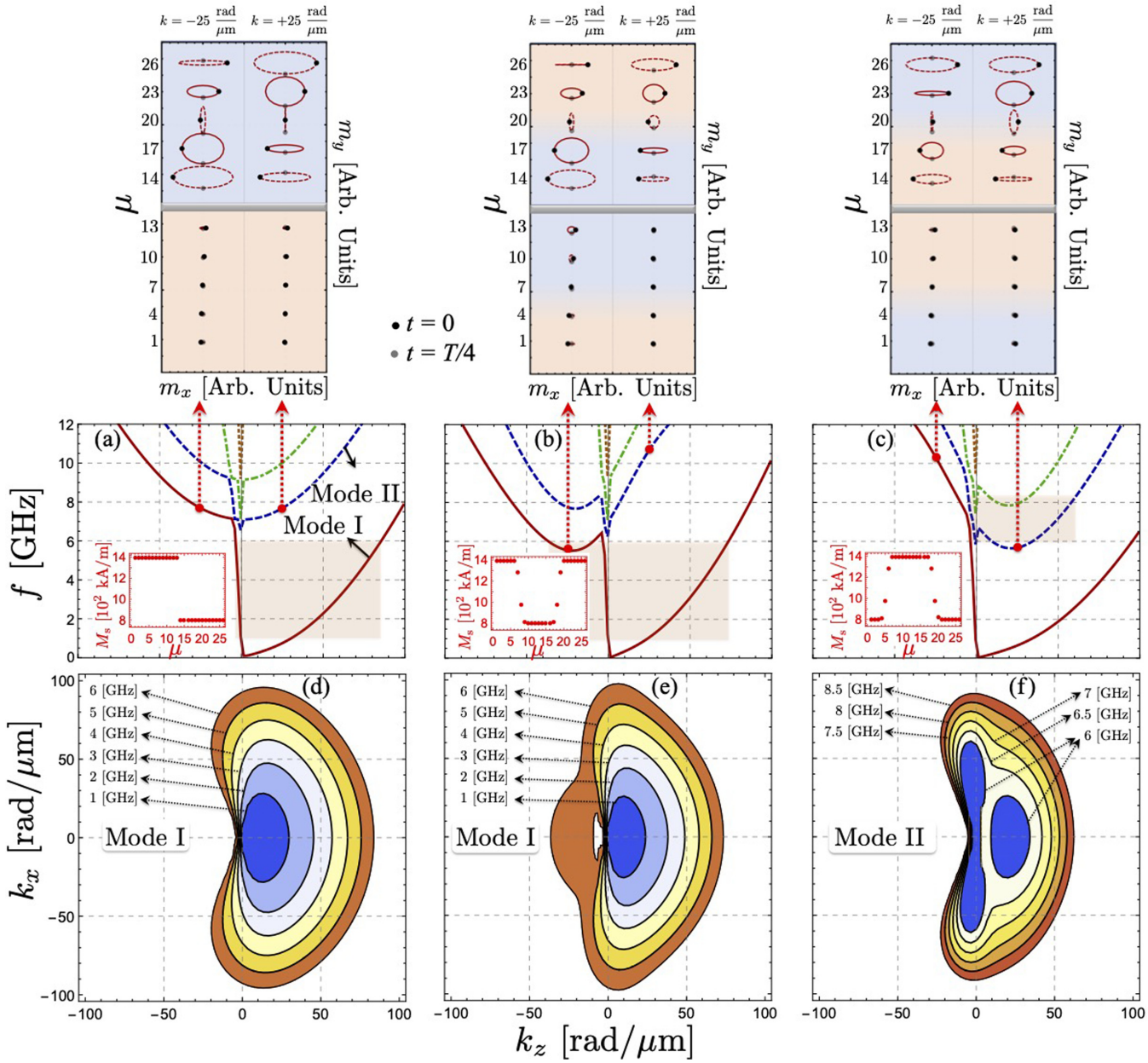

FIG. 5. (a) The dispersion relation of a typical bilayer Co/NM/Py system is shown. (b, c) The dispersion of a bilayer with the graduation of the saturation magnetization is depicted. The insets in (a–c) illustrate the saturation magnetization as a function of the thickness. Upper plots illustrate the SW profiles calculated at $k = \pm 25$ rad/μm. (d, e) The isofrequencies of mode I are shown. (f) The isofrequency curves are given for mode II. The shaded areas in (a–c) illustrate the range of frequencies used to calculate the isofrequency curves in (d–f). The thickness of both the Co and Py layers is 60 nm, where each FM layer has been divided into 13 sublayers.

of the other high-frequency modes) corresponds to an excitation of the upper FM layer. Therefore, such mode has the same energy for the two counterpropagating waves, since if the excitation is given only in one FM layer, the symmetry along the thickness is not broken, and therefore SWs propagating along $+z$ and $-z$ have the same dynamic energy or frequency. Now, under a different profile of variation of the saturation magnetization [see Figs. 5(b) and 5(c)], the dispersion is not significantly modified at frequencies lower than 5 GHz, so that the degree of the SW focalization of the fundamental mode is similar either with or without graduation of M_s. Nevertheless, the high-frequency modes are clearly modified, being nonreciprocal when the saturation magnetization varies along the thickness. Because the mode is mainly excited in one layer, it is expected that the variation of M_s induces nonreciprocity of the SWs since now the symmetry is broken along the thickness where the amplitude of the magnetization oscillations is remarkable. Figures 5(d) and 5(e) depict the isofrequency curves of mode I. Here, we see that mode I has similar focalization characteristics at low frequencies (lower than 5 GHz), even when the saturation magnetization has been varied across the thickness. This behavior is in concordance with the slight modification of the nonreciprocal properties of mode I. Nevertheless, the isofrequency curves change at high

frequencies because the second mode reduces its frequency at $+k$ or $-k$ depending on the type of graduation. This effect is observed in Fig. 5(e), where at 6 GHz the isofrequency curve is modified at negative wave vectors since the fundamental mode hybridizes with mode II. The isofrequency curves of mode II are shown in Fig. 5(f), where one can see that the nonreciprocity of the mode strongly influences its focusing properties. For instance, at 6 GHz, the curves depicted for mode II indicate that it is possible to create nontrivial interference patterns since spin waves with different wavelengths are propagating at the same frequency [25].

It is worth mentioning that the results presented in Fig. 5 are not notoriously modified if the magnetization profile changes abruptly or gradually (not shown). Namely, if a gradual (abrupt) magnetization change is considered in Fig. 5(a) [Figs. 5(b) and 5(c)], the SW dispersion does not significantly change, unless the magnetization graduation is extended along the whole thickness.

Overall, it is observed that magnetic graduation can be an essential ingredient in controlling the spin-wave focalization. In realistic materials, such magnetic graduation can be implemented in multilayered structures [79–85], in which extended interfaces are created by either directly tuning the thicknesses of the magnetic layers [80,82,83] or by interdiffusion via heat treatment [79,81,84,85]. Also, over the last few years, the realization of vertically graded thin films has been achieved in epitaxial compositionally graded alloy films, where graduation of the exchange strength [86], and saturation magnetization [87], can be induced along the thickness. Here, the synthesis are performed at room temperature by sputtering deposition [86–88], while the graded layers are fabricated by co-sputtering, keeping the power of one material fixed while changing that of the other to achieve the intended composition profile [86–88].

C. Micromagnetic simulations

The cases illustrated above show that synthetic antiferromagnets can be very versatile in generating highly focused waves, exhibiting more affluent propagation properties than other nonreciprocal systems, like heavy-metal/ferromagnet alloys. Indeed, the magnetic anisotropies (uniaxial, shape, surface, etc.), bilinear interlayer exchange, biquadratic interlayer exchange, thicknesses of the layers, and other properties can induce notable changes in the SW propagation and, hence, in its transfer of angular momentum and energy. Besides, the frequencies of the optic and acoustic modes have different focusing properties, despite that the frequency asymmetry is similar in magnitude for both modes (at least in the low wave-vector range). Also, in some cases, there is a frequency range where only the excitation of the low-frequency mode is given, while at high frequencies, more than one mode is excited at the same frequency. Thus, in general, the propagation of the waves around a point-source excitation can be channeled with the properties of one or more modes, and therefore, nontrivial spin-wave flow can be obtained. To illustrate this effect, we have performed micromagnetic simulations using the GPU-accelerated code MUMAX3 [89] for a bilayer system stabilized with an interlayer exchange constant of $J_{\text{inter}} = -1$ mJ/m^2, while the Co layer has a uniaxial anisotropy field of $\mu_0 H_{\text{u}} = 15$ mT. Two bilayers with different thicknesses are used, namely, Co(10 nm)NM(5 nm)Py(5 nm) and Co(30 nm)NM(5 nm)Py(15 nm). Note that we have used different parameters than the previous discussion to make the simulations more efficient. The dispersion was computed for a bilayer system with $L = 10$ μm and $w = 256$ nm lateral extensions, for both considered cases. The magnetization dynamics was excited by applying a perpendicular external microwave field pulse, namely,

$$\mu_0 H_{\text{pulse}}(z,t) = \mu_0 H_{\text{pulse}}\ \text{sinc}(k_{\text{max}} z)\ \text{sinc}[2\pi f_{\text{max}}(t - t_0)] \tag{3}$$

with $\mu_0 H_{\text{pulse}} = 1$ T, a cutoff frequency $f_{\text{max}} = 50$ GHz, and the cutoff wave vector of $k_{\text{max}} = \pi N_z/L$, with N_z representing the number of considered cells along the length L. The coordinate system is the same as used in Fig. 1. The magnetization dynamic is calculated for a duration of 25 ns and sampled every 10 ps. The dispersion map is then obtained by summing up the Fourier transform in time and space along line scans in the z direction. For the simulation of the spin-wave profiles, a pointlike antenna excitation was used with a 20-nm spot size. A sinusoidal rf field was used with an amplitude of $\mu_0 H_{\text{rf}} = 0.1$ mT. A 5 μm $\times$ 5 μm computational box was used for the simulations between 5 and 50 GHz, while for the lower-frequency cases, due to the large wavelength of the spin waves, the considered computational box was doubled. The results for the case Co(10 nm)NM(5 nm)Py(5 nm) are depicted in Fig. 6. According to Fig. 6(a), where the lines are the theoretical calculations, and color codes are the simulations, there is a particular frequency f_{02} from which both modes (modes I and II) are excited. In contrast, below this common frequency (f_{02}), the spin-wave propagation can only have the features of the low-frequency mode (mode I) in the range of frequencies between f_{01} and f_{02}. Note that in the current example, both frequencies (f_{01} and f_{02}) that define the minimum of both modes are given at zero wave vector; nevertheless, this is not a general behavior because, under given conditions, these minima can be found at finite wave vectors [32,50]. Figures 6(b)–(f) show the isofrequency curves for 5, 10, 15, 20, and 35 GHz, while the upper panels of each plot depict the results of the micromagnetic simulations. The group velocity is indicated along each constant-frequency curve. For $f = 5$ GHz [see Fig. 6(b)], the calculations predict an asymmetric interference pattern along the z axis, where a more remarkable interference of the waves is expected along the $+z$ direction. This behavior is evidenced in the micromagnetic simulations, where the interference patterns along $+z$ and $-z$ are notoriously different. Here, the snapshots of the SW profiles are taken after 200 oscillation periods for every simulated frequency. As an initial magnetization state, the last obtained state of the previous frequency is taken to ensure that after 100 periods, the system is already in a dynamic stable state (see details in Ref. [90]). At frequencies of 10 and 15 GHz, focalized waves appear and, hence, there is a focused propagation of the waves along the $-z$ direction. Note that for 5, 10, and 15 GHz, the excitation of the waves is given at $f_{01} > f > f_{02}$, so that only mode I is involved in the analysis. At 20 GHz, the situation changes since now the second frequency mode is also excited [see Fig. 6(a)] and, hence, the propagation characteristics of the spin waves are

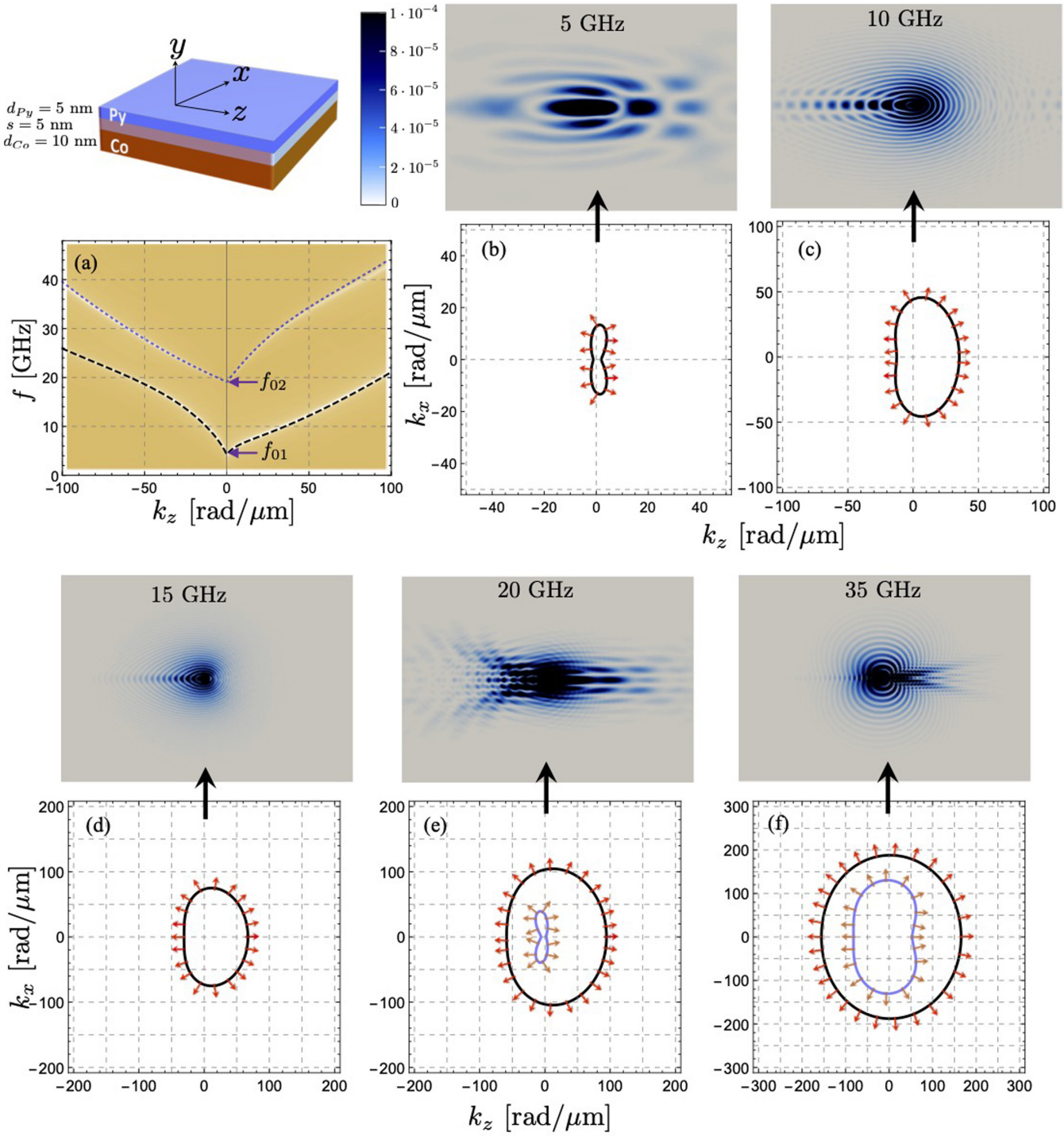

FIG. 6. (a) The dispersion relation of the Co(10 nm)NM(5 nm)Py(5 nm) system is shown (lines are solutions of the dynamic matrix method and color code represents the micromagnetic simulations). (b–f) The calculated isofrequencies curves are depicted. The upper panels in (b–f) illustrate the micromagnetic simulations. The group velocity is indicated along each isofrequency curve.

influenced by both modes. While mode I tends to create waves focused on $-z$, the second mode induces waves with larger wavelengths and interference patterns along both $+z$ and $-z$ directions. Thus, the resulting wave pattern is more complex as shown in the upper panel of Fig. 6(e). At higher frequencies, there is a superposition of both waves wherein, according to Fig. 6(f), the focusing properties are more influenced by the high-frequency mode, since the low-frequency mode is excited at larger wave vectors where the exchange interaction dominates, and the curve tends to be circular.

On the other side, the example Co(30 nm)NM(5 nm)Py(15 nm) is illustrated in Fig. 7. Overall, the behavior is similar to the previous case [Co(10 nm)NM(5 nm)Py(5 nm)]; nonetheless, because the nonreciprocity is stronger, there are also some differences in the focusing properties. While at 5 GHz, the behavior

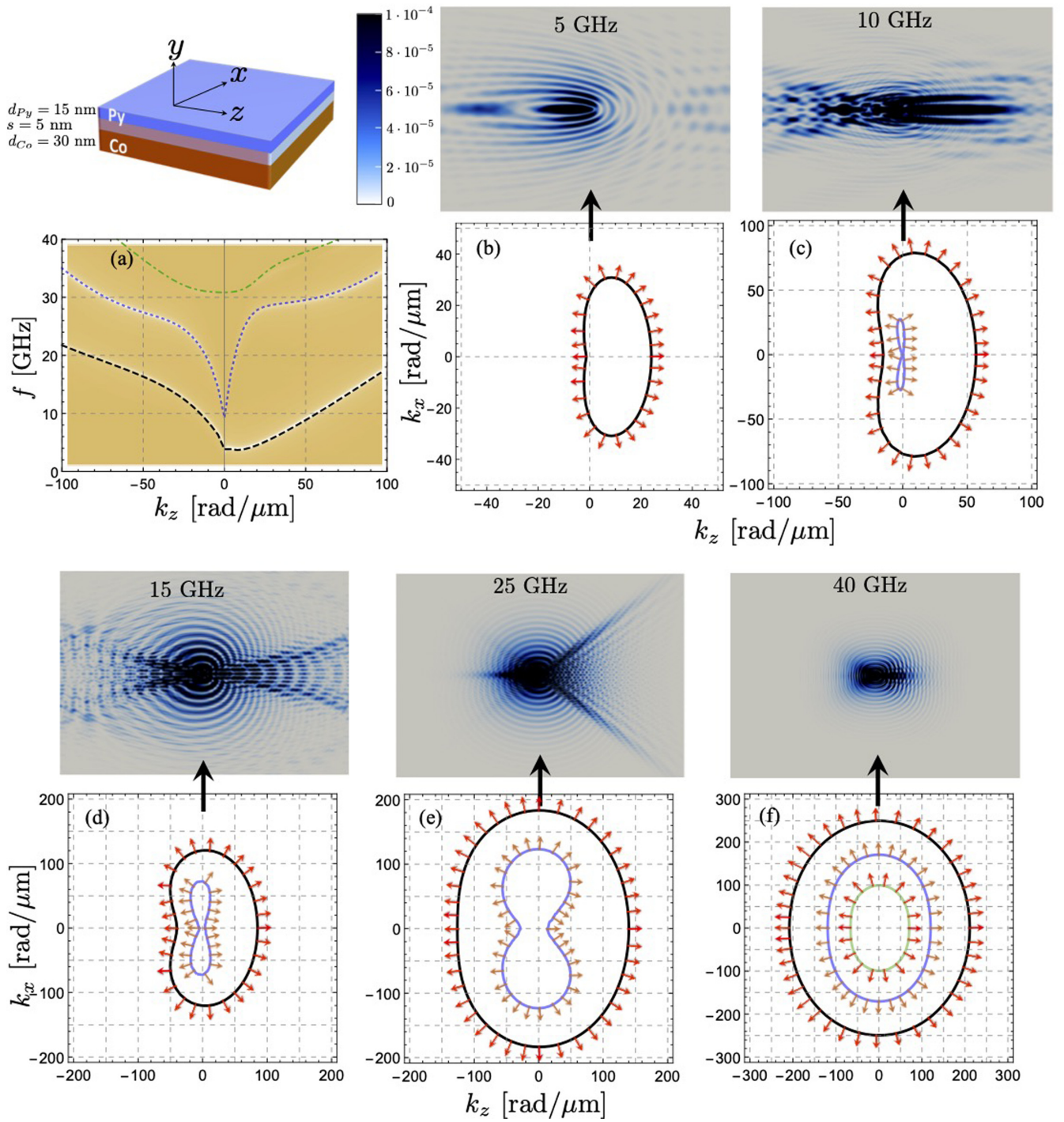

FIG. 7. SW properties obtained for Co(10 nm)NM(5 nm)Py(5 nm) system. (b–f) The isofrequency curves together with the respective micromagnetic simulations. The direction of the group velocity is indicated along each isofrequency curve.

is similar to Co(10 nm)NM(5 nm)Py(5 nm), at higher frequencies, we observe that the second mode influences the SW focalization in a broader range of frequencies. This is observed in the cases shown in Figs. 7(c)–(e). In the particular case of $f = 10$ GHz, SWs are channeled along the z axis, resulting from both modes that have clear zones in the isofrequency curve that focalize the group velocity and, hence, the energy of the wave. At higher frequencies, most of the modes are excited at more significant wave vectors so that the exchange dominates, resulting in a more negligible focusing effect [see Fig. 7(f)].

IV. CONCLUSIONS

We have theoretically addressed the focusing spin-wave properties for synthetic antiferromagnets. By analyzing the isofrequency curves, we have observed that the bilayer systems show a focalized spin-wave propagation when such

waves are excited by a single point source. We have analyzed the role of magnetic layer thicknesses and magnetic grading on focusing properties, and, as a general result, we have seen that the focalization characteristics of the fundamental and high-frequency modes are entirely different. By depending on the frequency range, it is possible to create highly focused spin waves where the focalization properties are only influenced by the low-frequency mode. In contrast, the focusing properties of the high-frequency modes are a superposition of more than one mode, exhibiting thus a more complex propagation. Finally, we can conclude that bilayer systems are excellent candidates for inducing and controlling highly focused spin waves and nonreciprocal interference patterns, which are essential for a new generation of magnonic devices such as demultiplexers, circulators, and isolators.

ACKNOWLEDGMENTS

The authors acknowledge financial support from Fondecyt, Grants No. 11170736, No. 1210607, and No. 1201153, and Basal Program for Centers of Excellence, Grant No. AFB180001 CEDENNA, CONICYT. P.A.-S. acknowledges the support of CONICYT 22201272, and PIIC No. 043/2020. Fruitful discussions with T. Schneider and A. Roldán-Molina are gratefully acknowledged. We also acknowledge the valuable comments of Lorenzo Fallarino about the graded magnetic materials.

APPENDIX: EFFECTIVE FIELDS OF DIPOLAR AND INTERLAYER EXCHANGE INTERACTIONS

The effective field $\mathbf{H}^{\mu}_{\text{eff}}$ can have different contributions, depending on which interactions are taken into account. Here we describe the effective fields associated with the dipolar and exchange interactions. For this purpose, it is useful to introduce a right-handed orthonormal basis $(\hat{\mathbf{x}}, \hat{\mathbf{y}}, \hat{\mathbf{z}})$ such that $\hat{\mathbf{y}}$ is normal to every layer and points in the direction of increasing μ. With respect to this basis, the volume V_μ of the μth layer can be written as $\mathbb{R} \times d_\mu \times \mathbb{R}$, where d_μ denotes the open interval (y_1^μ, y_2^μ) that describes the width of the μth layer.

1. Dipolar interaction

The magnetic potential due to the magnetization distribution is given by

$$\phi(\mathbf{r},t) = \frac{1}{4\pi}\sum_{\nu=1}^{N}\left[\oint_{\partial V_\nu} d\mathbf{S}' \cdot \frac{\mathbf{M}^\nu(\mathbf{r}',t)}{|\mathbf{r}-\mathbf{r}'|} - \int_{V_\nu} dV' \frac{\nabla'\cdot\mathbf{M}^\nu(\mathbf{r}',t)}{|\mathbf{r}-\mathbf{r}'|}\right], \tag{A1}$$

which, by the divergence theorem and the fact that $\nabla|\mathbf{r}-\mathbf{r}'| = -\nabla'|\mathbf{r}-\mathbf{r}'|$, can be rewritten as

$$\phi(\mathbf{r},t) = -\frac{1}{4\pi}\sum_{\nu=1}^{N}\int_{V_\nu} dV' \nabla\cdot\frac{\mathbf{M}^\nu(\mathbf{r}',t)}{|\mathbf{r}-\mathbf{r}'|}.$$

Since we are only interested in the dynamic effects, we drop the equilibrium term and make the substitution $\mathbf{M}^\nu \mapsto \mathbf{m}^\nu e^{i(\mathbf{k}\cdot\mathbf{r}-\omega t)}$; it follows that

$$\phi(\mathbf{r},t) = -\frac{1}{4\pi}\sum_{\nu=1}^{N}\nabla\left(\int_{V_\nu} dV' \frac{e^{i(\mathbf{k}\cdot\mathbf{r}-\omega t)}}{|\mathbf{r}-\mathbf{r}'|}\right)\cdot\mathbf{m}^\nu.$$

If $a, b, c \in \mathbb{R}$, then

$$\int_{-\infty}^{\infty}\int_{-\infty}^{\infty} dxdz \frac{e^{i(ax+bz)}}{\sqrt{x^2+z^2+c^2}} = 2\pi\frac{e^{-|c|\sqrt{a^2+b^2}}}{\sqrt{a^2+b^2}}.$$

Then, by using the previous identity to integrate over the xz plane, the potential can be further reduced to

$$\phi(\mathbf{r},t) = -\frac{1}{2k}\sum_{\nu}\nabla\left(e^{i(\mathbf{k}\cdot\mathbf{r}-\omega t)}\int_{d_\nu} dy' e^{-kQ}\right)\cdot\mathbf{m}^\nu,$$

where $\mathbf{Q} = \mathbf{P}\cdot(\mathbf{r}-\mathbf{r}')$ and $\mathbf{P} = \hat{\mathbf{y}}\otimes\hat{\mathbf{y}}$.

The effective dipolar field acting over the μth layer is defined as the average field over the layer's thickness. Namely, $\mathbf{H}^\mu(\mathbf{r},t) = -\frac{1}{|d_\mu|}\int_{d_\mu} dy \nabla\phi(\mathbf{r},t)$. Since $\mathbf{h}^\mu = \sum_{\nu=1}^{N}\mathbf{\Lambda}^{\mu\nu}\cdot\mathbf{m}^\nu$, we can make the identification

$$\mathbf{\Lambda}^{\mu\nu} = \frac{e^{-i\mathbf{k}\cdot\mathbf{r}}}{2k|d_\mu|}\int_{d_\mu} dy(\nabla\otimes\nabla)\left(e^{i\mathbf{k}\cdot\mathbf{r}}\int_{d_\nu} dy' e^{-kQ}\right).$$

In particular, if $\mu \neq \nu$, then

$$\mathbf{\Lambda}^{\mu\nu} = \frac{e^{-kQ}}{2k^3|d_\mu|}\left(\mathbf{k}\otimes\mathbf{k} + ik\frac{\mathbf{k}\otimes\mathbf{Q}+\mathbf{Q}\otimes\mathbf{k}}{Q} - k^2\frac{\mathbf{Q}\otimes\mathbf{Q}}{Q^2}\right)\Bigg|_{y'=y_1^\nu}^{y_2^\nu}\Bigg|_{y=y_1^\mu}^{y_2^\mu},$$

where $\mathbf{Q}/Q$ behaves like $\text{sgn}(\mu-\nu)\hat{\mathbf{y}}$ after the evaluation. If $\mu = \nu$, then

$$\mathbf{\Lambda}^{\mu\mu} = \frac{1-e^{-k|d_\mu|}}{k|d_\mu|}\left(\frac{\mathbf{k}\otimes\mathbf{k}}{k^2} - \hat{\mathbf{y}}\otimes\hat{\mathbf{y}}\right) - \frac{\mathbf{k}\otimes\mathbf{k}}{k^2}.$$

Then, with the elements $\mathbf{\Lambda}^{\mu\nu}$ in hand, it is straightforward to obtain the effective dynamic fields of dipolar origin.

2. Interlayer exchange field

To model the interlayer exchange interaction we use the energy density as follows:

$$\epsilon^{\text{ex}} = \frac{1}{2}\sum_{\mu,\nu=1}^{N}\frac{J_{\text{intra}}}{M_s^\mu M_s^\nu}\mathbf{M}^\mu\cdot\mathbf{M}^\nu(\delta_{\mu,\nu+1}+\delta_{\mu,\nu-1}) + \frac{J_{\text{inter}}-J_{\text{intra}}}{M_s^\mu M_s^\nu}\mathbf{M}^\alpha\cdot\mathbf{M}^{\alpha+1},$$

where α denotes the interface between the two films, so that the layers α and $\alpha+1$ correspond to the ones in contact with the nonmagnetic film. Because $\mathbf{h}^\mu = \sum_{\nu=1}^{N}\mathbf{\Lambda}_{\text{ex}}^{\mu\nu}\cdot\mathbf{m}^\nu$, it follows that $\mathbf{\Lambda}_{\text{ex}}^{\mu\nu} = \Psi_{\nu,\mu}\mathbf{I}$, where $\mathbf{I}$ is the identity and

$$\Psi_{\nu,\mu} = -\frac{1}{2d_\mu}\frac{J_{\text{intra}}}{\mu_0 M_s^\mu M_s^\nu}(\delta_{\mu,\nu+1}+\delta_{\mu,\nu-1}) - \frac{1}{d_\mu}\frac{J_{\text{inter}}-J_{\text{intra}}}{\mu_0 M_s^\mu M_s^\nu}(\delta_{\alpha,\mu}\delta_{\alpha+1,\nu}+\delta_{\alpha+1,\mu}\delta_{\alpha,\nu}).$$

[1] M. Berry and C. Upstill, *IV Catastrophe Optics: Morphologies of Caustics and Their Diffraction Patterns* (Elsevier, Amsterdam, 1980), pp. 257–346.

[2] Y. A. Kravtsov and Y. I. Orlov, *Caustics, Catastrophes and Wave Fields* (Springer, Berlin, 1993).

[3] L. Froehly, F. Courvoisier, A. Mathis, M. Jacquot, L. Furfaro, R. Giust, P. A. Lacourt, and J. M. Dudley, Opt. Express **19**, 16455 (2011).

[4] A. Tanaka, Phys. Rev. Lett. **80**, 1414 (1998).

[5] C. Charmousis, V. Onemli, Z. Qiu, and P. Sikivie, Phys. Rev. D **67**, 103502 (2003).

[6] A. I. Harte and T. D. Drivas, Phys. Rev. D **85**, 124039 (2012).

[7] K. Pasmatsiou, Phys. Rev. D **97**, 036008 (2018).

[8] V. T. Buchwald, Q. J. Mech. Appl. Math. **14**, 293 (1961).

[9] G. A. Northrop and J. P. Wolfe, Phys. Rev. B **22**, 6196 (1980).

[10] P. Taborek and D. Goodstein, Solid State Commun. **33**, 1191 (1980).

[11] R. E. Camley and A. A. Maradudin, Phys. Rev. B **27**, 1959 (1983).

[12] A. G. Every, Phys. Rev. B **34**, 2852 (1986).

[13] I. Epstein and A. Arie, Phys. Rev. Lett. **112**, 023903 (2014).

[14] X. Shi, X. Lin, F. Gao, H. Xu, Z. Yang, and B. Zhang, Phys. Rev. B **92**, 081404(R) (2015).

[15] J. Spector, H. L. Stormer, K. W. Baldwin, L. N. Pfeiffer, and K. W. West, Appl. Phys. Lett. **56**, 1290 (1990).

[16] V. V. Cheianov, V. Fal'ko, and B. L. Altshuler, Science **315**, 1252 (2007).

[17] J. Cserti, A. Pályi, and C. Péterfalvi, Phys. Rev. Lett. **99**, 246801 (2007).

[18] V. Krivoruchko and A. Savchenko, Acta Phys. Pol. A **133**, 463 (2018).

[19] V. Veerakumar and R. E. Camley, Phys. Rev. B **74**, 214401 (2006).

[20] V. E. Demidov, S. O. Demokritov, D. Birt, B. O'Gorman, M. Tsoi, and X. Li, Phys. Rev. B **80**, 014429 (2009).

[21] T. Schneider, A. A. Serga, A. V. Chumak, C. W. Sandweg, S. Trudel, S. Wolff, M. P. Kostylev, V. S. Tiberkevich, A. N. Slavin, and B. Hillebrands, Phys. Rev. Lett. **104**, 197203 (2010).

[22] S. Mansfeld, J. Topp, K. Martens, J. N. Toedt, W. Hansen, D. Heitmann, and S. Mendach, Phys. Rev. Lett. **108**, 047204 (2012).

[23] T. Sebastian, T. Brächer, P. Pirro, A. A. Serga, B. Hillebrands, T. Kubota, H. Naganuma, M. Oogane, and Y. Ando, Phys. Rev. Lett. **110**, 067201 (2013).

[24] R. Gieniusz, H. Ulrichs, V. D. Bessonov, U. Guzowska, A. I. Stognii, and A. Maziewski, Appl. Phys. Lett. **102**, 102409 (2013).

[25] J.-V. Kim, R. L. Stamps, and R. E. Camley, Phys. Rev. Lett. **117**, 197204 (2016).

[26] F. Heussner, A. A. Serga, T. Brächer, B. Hillebrands, and P. Pirro, Appl. Phys. Lett. **111**, 122401 (2017).

[27] J. J. Bible and R. E. Camley, Phys. Rev. B **95**, 224412 (2017).

[28] F. Heussner, G. Talmelli, M. Geilen, B. Heinz, T. Brächer, T. Meyer, F. Ciubotaru, C. Adelmann, K. Yamamoto, A. A. Serga, B. Hillebrands, and P. Pirro, Phys. Status Solidi RRL **14**, 1900695 (2020).

[29] S. O. Demokritov, *Spin Wave Confinement: Propagating Waves*, 2nd ed. (Pan Stanford, Singapore, 2017), pp. 219–260.

[30] X. Xing and Y. Zhou, NPG Asia Mater. **8**, e246 (2016).

[31] M. Garst, J. Waizner, and D. Grundler, J. Phys. D: Appl. Phys. **50**, 293002 (2017).

[32] V. Sluka, T. Schneider, R. A. Gallardo, A. Kákay, M. Weigand, T. Warnatz, R. Mattheis, A. Roldán-Molina, P. Landeros, V. Tiberkevich, A. Slavin, G. Schütz, A. Erbe, A. Deac, J. Lindner, J. Raabe, J. Fassbender, and S. Wintz, Nat. Nanotechnol. **14**, 328 (2019).

[33] X. Xing, Y. Zhou, and H. B. Braun, Phys. Rev. Appl. **13**, 034051 (2020).

[34] A. Barman, G. Gubbiotti, S. Ladak, A. O. Adeyeye, M. Krawczyk, J. Gräfe, C. Adelmann, S. Cotofana, A. Naeemi, V. I. Vasyuchka, B. Hillebrands, S. A. Nikitov, H. Yu, D. Grundler, A. V. Sadovnikov, A. A. Grachev, S. E. Sheshukova, J.-Y. Duquesne, M. Marangolo, G. Csaba, W. Porod, V. E. Demidov, S. Urazhdin, S. O. Demokritov, E. Albisetti, D. Petti, R. Bertacco, H. Schultheiss, V. V. Kruglyak, V. D. Poimanov, S. Sahoo, J. Sinha, H. Yang, M. Münzenberg, T. Moriyama, S. Mizukami, P. Landeros, R. A. Gallardo, G. Carlotti, J.-V. Kim, R. L. Stamps, R. E. Camley, B. Rana, Y. Otani, W. Yu, T. Yu, G. E. W. Bauer, C. Back, G. S. Uhrig, O. V. Dobrovolskiy, B. Budinska, H. Qin, S. van Dijken, A. V. Chumak, A. Khitun, D. E. Nikonov, I. A. Young, B. W. Zingsem, and M. Winklhofer, J. Phys.: Condens. Matter **33**, 413001 (2021).

[35] K. Di, V. L. Zhang, H. S. Lim, S. C. Ng, M. H. Kuok, J. Yu, J. Yoon, X. Qiu, and H. Yang, Phys. Rev. Lett. **114**, 047201 (2015).

[36] J. Cho, N.-H. Kim, S. Lee, J.-S. Kim, R. Lavrijsen, A. Solignac, Y. Yin, D.-S. Han, N. J. J. van Hoof, H. J. M. Swagten, B. Koopmans, and C.-Y. You, Nat. Commun. **6**, 7635 (2015).

[37] H. T. Nembach, J. M. Shaw, M. Weiler, E. Jue, and T. J. Silva, Nat. Phys. **11**, 825 (2015).

[38] M. Belmeguenai, J.-P. Adam, Y. Roussigné, S. Eimer, T. Devolder, J.-V. Kim, S. M. Cherif, A. Stashkevich, and A. Thiaville, Phys. Rev. B **91**, 180405(R) (2015).

[39] A. K. Chaurasiya, C. Banerjee, S. Pan, S. Sahoo, S. Choudhury, J. Sinha, and A. Barman, Sci. Rep. **6**, 32592 (2016).

[40] S. Tacchi, R. E. Troncoso, M. Ahlberg, G. Gubbiotti, M. Madami, J. Åkerman, and P. Landeros, Phys. Rev. Lett. **118**, 147201 (2017).

[41] R. A. Gallardo, D. Cortés-Ortuño, R. E. Troncoso, and P. Landeros, in *Three-Dimensional Magnonics* (Jenny Stanford Publishing, Berlin, 2019), pp. 121–160.

[42] M. Kataoka, J. Phys. Soc. Jpn. **56**, 3635 (1987).

[43] D. Cortés-Ortuño and P. Landeros, J. Phys: Condens. Matter **25**, 156001 (2013).

[44] Y. Iguchi, S. Uemura, K. Ueno, and Y. Onose, Phys. Rev. B **92**, 184419 (2015).

[45] S. Seki, Y. Okamura, K. Kondou, K. Shibata, M. Kubota, R. Takagi, F. Kagawa, M. Kawasaki, G. Tatara, Y. Otani, and Y. Tokura, Phys. Rev. B **93**, 235131 (2016).

[46] T. Weber, J. Waizner, G. S. Tucker, L. Beddrich, M. Skoulatos, R. Georgii, A. Bauer, C. Pfleiderer, M. Garst, and P. Böni, AIP Adv. **8**, 101328 (2018).

[47] T. J. Sato and K. Matan, J. Phys. Soc. Jpn. **88**, 081007 (2019).

[48] J. A. Otálora, M. Yan, H. Schultheiss, R. Hertel, and A. Kákay, Phys. Rev. Lett. **117**, 227203 (2016).

[49] D. D. Sheka, O. V. Pylypovskyi, P. Landeros, Y. Gaididei, A. Kákay, and D. Makarov, Commun. Phys. **3**, 128 (2020).

[50] R. A. Gallardo, P. Alvarado-Seguel, T. Schneider, C. Gonzalez-Fuentes, A. Roldán-Molina, K. Lenz, J. Lindner, and P. Landeros, New J. Phys. **21**, 033026 (2019).

[51] K. Mika and P. Grünberg, Phys. Rev. B **31**, 4465 (1985).

[52] P. Grünberg, J. Appl. Phys. **57**, 3673 (1985).

[53] P. Grünberg, R. Schreiber, Y. Pang, M. B. Brodsky, and H. Sowers, Phys. Rev. Lett. **57**, 2442 (1986).

[54] P. X. Zhang and W. Zinn, Phys. Rev. B **35**, 5219 (1987).

[55] G. Binasch, P. Grünberg, F. Saurenbach, and W. Zinn, Phys. Rev. B **39**, 4828 (1989).

[56] J. Barnaś and P. Grünberg, J. Magn. Magn. Mater. **82**, 186 (1989).

[57] R. A. Gallardo, T. Schneider, A. K. Chaurasiya, A. Oelschlägel, S. S. P. K. Arekapudi, A. Roldán-Molina, R. Hübner, K. Lenz, A. Barman, J. Fassbender, J. Lindner, O. Hellwig, and P. Landeros, Phys. Rev. Appl. **12**, 034012 (2019).

[58] E. Albisetti, S. Tacchi, R. Silvani, G. Scaramuzzi, S. Finizio, S. Wintz, C. Rinaldi, M. Cantoni, J. Raabe, G. Carlotti, R. Bertacco, E. Riedo, and D. Petti, Adv. Mater. **32**, 1906439 (2020).

[59] M. Grassi, M. Geilen, D. Louis, M. Mohseni, T. Brächer, M. Hehn, D. Stoeffler, M. Bailleul, P. Pirro, and Y. Henry, Phys. Rev. Appl. **14**, 024047 (2020).

[60] A. F. Franco and P. Landeros, Phys. Rev. B **102**, 184424 (2020).

[61] K. Di, S. X. Feng, S. N. Piramanayagam, V. L. Zhang, H. S. Lim, S. C. Ng, and M. H. Kuok, Sci. Rep. **5**, 10153 (2015).

[62] P. Alvarado-Seguel and R. A. Gallardo, Phys. Rev. B **100**, 144415 (2019).

[63] R. Verba, V. Tiberkevich, E. Bankowski, T. Meitzler, G. Melkov, and A. Slavin, Appl. Phys. Lett. **103**, 082407 (2013).

[64] R. Camley, Surf. Sci. Rep. **7**, 103 (1987).

[65] J. Lan, W. Yu, R. Wu, and J. Xiao, Phys. Rev. X **5**, 041049 (2015).

[66] N. Reiskarimian and H. Krishnaswamy, Nat. Commun. **7**, 11217 (2016).

[67] D. L. Sounas and A. Alù, Nat. Photonics **11**, 774 (2017).

[68] M. Ishibashi, Y. Shiota, T. Li, S. Funada, T. Moriyama, and T. Ono, Sci. Adv. **6**, aaz6931 (2020).

[69] M. Grimsditch, L. Giovannini, F. Montoncello, F. Nizzoli, G. K. Leaf, and H. G. Kaper, Phys. Rev. B **70**, 054409 (2004).

[70] L. Giovannini, F. Montoncello, F. Nizzoli, G. Gubbiotti, G. Carlotti, T. Okuno, T. Shinjo, and M. Grimsditch, Phys. Rev. B **70**, 172404 (2004).

[71] Y. Henry, O. Gladii, and M. Bailleul, arXiv:1611.06153.

[72] J. Wei, Z. Zhu, C. Song, H. Feng, P. Jing, X. Wang, Q. Liu, and J. Wang, J. Phys. D: Appl. Phys. **49**, 265002 (2016).

[73] M. Pousthomis, E. Anagnostopoulou, I. Panagiotopoulos, R. Boubekri, W. Fang, F. Ott, K. A. Atmane, J. Y. Piquemal, L. M. Lacroix, and G. Viau, Nano Res. **8**, 2231 (2015).

[74] H. Yu, G. Duerr, R. Huber, M. Bahr, T. Schwarze, F. Brandl, and D. Grundler, Nat. Commun. **4**, 2702 (2013).

[75] M. Krawczyk and D. Grundler, J. Phys.: Condens. Matter **26**, 123202 (2014).

[76] I. Bertelli, J. J. Carmiggelt, T. Yu, B. G. Simon, C. C. Pothoven, G. E. Bauer, Y. M. Blanter, J. Aarts, and T. Van Der Sar, Sci. Adv. **6**, eabd3556 (2020).

[77] H. Yu, R. Huber, T. Schwarze, F. Brandl, T. Rapp, P. Berberich, G. Duerr, and D. Grundler, Appl. Phys. Lett. **100**, 262412 (2012).

[78] C. Liu, J. Chen, T. Liu, F. Heimbach, H. Yu, Y. Xiao, J. Hu, M. Liu, H. Chang, T. Stueckler, S. Tu, Y. Zhang, Y. Zhang, P. Gao, Z. Liao, D. Yu, K. Xia, N. Lei, W. Zhao, and M. Wu, Nat. Commun. **9**, 738 (2018).

[79] D. Goll, A. Breitling, L. Gu, P. A. van Aken, and W. Sigle, J. Appl. Phys. **104**, 083903 (2008).

[80] M. Marcellini, M. Pärnaste, B. Hjörvarsson, and M. Wolff, Phys. Rev. B **79**, 144426 (2009).

[81] T.-J. Zhou, B. C. Lim, and B. Liu, Appl. Phys. Lett. **94**, 152505 (2009).

[82] B. J. Kirby, S. M. Watson, J. E. Davies, G. T. Zimanyi, K. Liu, R. D. Shull, and J. A. Borchers, J. Appl. Phys. **105**, 07C929 (2009).

[83] B. J. Kirby, J. E. Davies, K. Liu, S. M. Watson, G. T. Zimanyi, R. D. Shull, P. A. Kienzle, and J. A. Borchers, Phys. Rev. B **81**, 100405(R) (2010).

[84] V. Alexandrakis, D. Niarchos, K. Mergia, J. Lee, J. Fidler, and I. Panagiotopoulos, J. Appl. Phys. **107**, 013903 (2010).

[85] J. S. Chen, L. S. Huang, J. F. Hu, G. Ju, and G. M. Chow, J. Phys. D: Appl. Phys. **43**, 185001 (2010).

[86] B. J. Kirby, H. F. Belliveau, D. D. Belyea, P. A. Kienzle, A. J. Grutter, P. Riego, A. Berger, and C. W. Miller, Phys. Rev. Lett. **116**, 047203 (2016).

[87] L. Fallarino, P. Riego, B. J. Kirby, C. W. Miller, and A. Berger, Materials **11**, 251 (2018).

[88] L. Fallarino, B. J. Kirby, and E. E. Fullerton, J. Phys. D: Appl. Phys. **54**, 303002 (2021).

[89] A. Vansteenkiste, J. Leliaert, M. Dvornik, M. Helsen, F. Garcia-Sanchez, and B. V. Waeyenberge, AIP Adv. **4**, 107133 (2014).

[90] K. Wagner, L. Körber, S. Stienen, J. Lindner, M. Farle, and A. Kákay, IEEE Magn. Lett. **12**, 1 (2021).